HHS Public Access

Author manuscript

Mol Psychiatry. Author manuscript; available in PMC 2017 February 24.

Published in final edited form as:

Mol Psychiatry. 2017 July ; 22(7): 990–1001. doi:10.1038/mp.2016.104.

A CNS-permeable Hsp90 inhibitor rescues synaptic dysfunction and memory loss in APP-overexpressing Alzheimer's mouse model via an HSF1-mediated mechanism

Bin Wang[1], **Yu Liu**[2], **Lianyan Huang**[3], **Jianjun Chen**[4,**], **Jing jing Li**[1], **Ruishan Wang**[1], **Eunhee Kim**[1], **Carles Justicia**[5], **Kazuko Sakata**[1], **Hao Chen**[1], **Anna Planas**[5], **Rennolds S Ostrom**[1], **Wei Li**[4], **Guang Yang**[3], **Michael P. McDonald**[2,7], **Ruihong Chen**[6], **Detlef Heck**[2], and **Francesca-Fang Liao**[1,*]

[1]Department of Pharmacology, University of Tennessee Health Science Center, College of Medicine, Memphis, Tennessee 38163

[2]Department of Anatomy & Neurobiology, University of Tennessee Health Science Center, College of Medicine, Memphis, Tennessee 38163

[3]Department of Anesthesiology, New York University School of Medicine, New York, NY 10016

[4]Department of Pharmaceutical Sciences, University of Tennessee Health Science Center, College of Medicine, Memphis, Tennessee 38163

[5]Department of Brain Ischemia and Neurodegeneration, Institute for Biomedical Research (IIBB-CSIC), Rossello 161, planta 6, 08036-Barcelona, Spain

[6]Oncosynergy, Inc; 409 Illinois St., San Francisco, CA, 94158

[7]Department of Neurology, University of Tennessee Health Science Center, College of Medicine, Memphis, Tennessee 38163

Abstract

Induction of neuroprotective heat-shock proteins via pharmacological Hsp90 inhibitors is currently being investigated as a potential treatment for neurodegenerative diseases. Two major hurdles for therapeutic use of Hsp90 inhibitors are systemic toxicity and limited CNS permeability. We demonstrate here that chronic treatment with a proprietary Hsp90 inhibitor compound (OS47720) not only elicits a heat shock-like response, but also offers synaptic protection in symptomatic Tg2576 mice, a model of Alzheimer's disease (AD), without noticeable systemic toxicity. Despite

*Correspondence should be addressed to Francesca-Fang Liao, Department of Pharmacology, University of Tennessee Health Science Center, College of Medicine, Memphis, Tennessee 38163. fliao@uthsc.edu.

**Current address: Department of Pharmaceutical Sciences, Chicago State University, College of Pharmacy, Chicago, IL 60628

Author contributions: F.-F.L. designed research; B. W., Y. L., L. H., J. C., J. L., R. W., E. K. and C. J. performed research; K. S., H. C., A. P., R. S. O., W. L., G. Y., M. P. M., D. H. and F.-F.L. analyzed data; R. C. provided compound and consultation; B.W., F.-F.L. wrote the paper.

CONFLICT OF INTEREST

The authors declare no conflict of interest.

Supplementary Information accompanies the paper on the *Molecular Psychiatry* website.

a short half-life of OS47720 in mouse brain, a single intraperitoneal injection induces rapid and long-lasting (> 3 d) nuclear activation of the heat shock factor, HSF1. Mechanistic study indicates that the remedial effects of OS47720 depend upon HSF1 activation and the subsequent HSF-1-mediated transcriptional events on synaptic genes. Taken together, this work reveals a novel role of HSF1 in synaptic function and memory, which likely occurs through modulation of the synaptic transcriptome.

Introduction

Alzheimer's disease (AD) is a progressive neurological disorder afflicting millions of individuals worldwide. Current therapeutic approaches focus on reducing Aβ levels via inhibiting β- and γ-secretases, but have yielded little success clinically[1, 2]. Heat shock protein 90 (Hsp90) is a molecular chaperone protein ubiquitously expressed throughout all tissues in the body. Some of its client proteins have been implicated in neurodegeneration. Thus, pharmacologically feasible Hsp90 inhibitors have been studied extensively in experimental conditions of neurodegenerative diseases[3, 4]. In most studies, the rationale has been premised on the presumed functions of Hsp90 inhibitors in harnessing other chaperone proteins to facilitate degradation of pathological proteins. The majority of the literature on Hsp90 describes data generated from *in vitro* studies, while *in vivo* success has been limited[5–9].

We have thus undertaken a different approach. While the two major chaperone proteins, Hsp70 and Hsp90, are both richly localized in synaptic compartments[10], little is known regarding their synaptic functions. Hsp90 inhibitors bind to the N-terminal ATP binding site, resulting in dissociation and subsequent degradation of its client proteins, which includes HSF1[11–13]. Upon Hsp90 inhibition, HSF1 is released and forms an active trimer that translocates to the nucleus. There, it binds to heat-shock response elements (HSEs) and transactivates numerous target genes (e.g., *hsp* and synaptic genes[14]). Here, we report on a CNS-permeable Hsp90 inhibitor (OS47720) that displays exceptional safety and efficacy acutely and chronically in a mouse model of AD. We also show that OS47720 strengthens synaptic function via HSF1-dependent transcriptional events (e.g., *bdnf* genes).

MATERIALS AND METHODS

Mice

All animal procedures were performed in accordance with the Animal Scientific Procedures Act and with the approval of the Institutional Animal Care and Use Committee (IACUC) at University of Tennessee Health Science Center (UTHSC). Tg2576 mice were originally purchased from Taconic (Stock#: 1394). The HSF1 heterozygous mice were purchased from the Jackson Lab (Stock #018582). The iHSP70-mPlum reporter mice were generated as described[18] and the work was performed in Spain via collaboration.

Primary neuron culture

Cortical and hippocampal neurons were isolated and purified from E17 embryos of Sprague Dawley (SD) rats as previously described[14].

Naturally secreted Aβ-containing conditioned medium

Conditioned medium (CM) containing naturally secreted Aβ oligomers were collected from cultures of 7PA2/CHO cells as previously described[14].

Chemical compounds/reagents

OS47720 (abbreviated as OS47720), was initially provided by NexGenenix Pharmaceutical, Inc., NY with an original name of NXD30020, later by OncoSynergy, San Francisco, CA. KRIBB11, KN92 and KN93 was purchased from Tocris; RpcAMP and H89 was purchased from Sigma; LY294002 was purchased from LC labs; U0126 was purchased from Cell signal.

Compounds administration

The solvent used for OS47720 administration consisted of 6% Dimethylacetamide (DMA), 5% Tween-80 and 89% sterile H_2O. Compound was injected intraperitoneally (IP) twice a week for the first 4 weeks, then three times a week until the end of study. Treatment started from 9-month of Tg2576 mice and lasted for 3 months or from 12-month of Tg2576 and lasted for 6 months.

Surgical procedures

Mice were anesthetized by intraperitoneal injection of xylazine/ketamine (13/87 mg/kg). Guide cannula (Plastics One) was implanted above the dorsal lateral ventricle using a stereotaxic instrument (KOPF Instruments) at the coordinates: AP=−0.37 mm; ML=+1.00 mm; DV=−1.5 mm with respect to bregma. Cannula was mounted to the skull with medical grade superglue (Loctite 454). A paired dummy was fitted into each cannula to prevent clogging. Intra-CA1 injection of viruses is similar to cannulation. Instead of implanting cannulae, we used KOPF microinjection unit (Model#: 5000) to inject 1 μl of AAV viruses into each of the CA1 region at the coordinates: AP=−2 mm; ML=+1.5 mm; DV=−1.75 mm with respect to bregma with respect to bregma, speed of 0.2 μl/min. Syringe will be remained for additional 3 min for drug diffuse. Compound administration and behavior tests started at least 5 days after surgery. Virus- injected mice were housed for 3 weeks before tests.

Liquid chromatography–mass spectrometry (LC-MS)

Brain tissues were collected at 1, 2, 6, and 24 hours following i.p administration of the compound. The brain samples (~250 mg/mouse) were collected and homogenized after the addition of 100 μl de-ionized water. The compounds in the brain homogenates were extracted with 0.9 ml acetonitrile and ice-cool for 20 min. The supernatants (700 μl) were transferred to a new vial, centrifuged, and dried under N_2. The dry samples were reconstituted into 140 μl of acetonitrile, mixed thoroughly, and centrifuged, the supernatant were used for LC-MS/MS analysis.

LC-MS/MS analysis was performed on an API-4500 triple-quadrupole system (AB Sciex, Foster City, CA) with a Turbo V ESI ion source. The spraying needle voltage was set as 5.5 kV for positive mode. Curtain gas was set at 10 psi, drying gas was set to 20 psi, nebulizing

gas was set at 20 psi, and CAD gas was set at 7 psi. The probe heater temperature was set at 400°C. Data acquisition and quantitative processing were accomplished by the Analyst software, version 1.6.1 (AB Sciex, Foster City, CA). Sample solution (5 μl) was injected into a Shimadzu (Canby, OR) Nexera UPLC system. Multiple reaction monitoring (MRM) mode, scanning m/z 457.0→194.1 (positive mode), was used to obtain the most sensitive signals. Chromatographic separation of the analytes was performed using a Luna PFP column (50×2.0 mm i.d, 3.0 μm particle size, Phenomenex, Torrance, CA) with a guard column, applying gradient elution. Mobile phase A: 0.01% formic acid in water; B: 0.01% formic acid in methanol. 0–0.5 min: 2% B, 0.5–0.6 min: 2–98% B; 0.6–4 min: 98% B; 4–4.3 min: 98–2% B; 4.3–5.0 min: 2% B. The flow rate was set to 0.3 ml/min.

In vivo imaging of dendritic spines and data analysis

The surgical procedure for chronic transcranial two-photon imaging and data analysis with NIH ImageJ software has been described previously[15]. Filopodia were identified as long, thin structures without enlarged heads and the rest of the protrusions were classified as spines. Spines were considered the same between two views based on their spatial relationship to adjacent landmarks and spines. Spines in the second view were considered different if they were more than 0.7 μm away from their expected positions based on the first view. More than 150 spines were analyzed from each animal to calculate spine formation and elimination. The rate of spine formation or elimination was calculated as the number of spines formed or eliminated divided by the number of spines existing in the first view.

In vivo recording of cortical-hippocampal network

Thirteen mice (B6, male, 18-month-old) were divided into OS47720 (n = 7) and vehicle (Veh, n = 6) treated groups (Supplementary Table 1). Animals were surgically prepared for unilateral intraventricular infusion (IVI) and awake head-fixed recordings of local field potentials (LFPs) from the contralateral hemisphere. The infusion of OS47720/Veh (2 μL) through an implanted cannula in lateral ventricle were completed over 10 min. LFPs in the CA1 region of the hippocampus and the prefrontal cortex (PFC) were recorded during three time-periods: 10-min-pre-IVI, 10-min-post-IVI and 1-day-post-IVI.

During LFP recording, the depths of recording position in CA1 were determined by the presence of the characteristic high-frequency ripple activity that was synchronous across the two recording sites. The recording locations were also confirmed by electrolytic lesions at the end of experiments and anatomical verification in Nissl stained sections. Each animal's breathing was continuously monitored through a thermistor positioned near one nostril. Breathing signals were used for offline LFP data selection. In the present study, data recorded during resting-state (i.e., a smooth breathing rhythm with a stable rhythm below 4 Hz) were selected for further analyses.

LFP data from the two electrodes in CA1 (separated by 0.3 mm) and the one in the PFC were selected for coherence analysis. Five continuous resting-state LFP signals (1-min each) were extracted from each of the three time-periods (pre-, immediately after IVI and one day after IVI) and exported as Matlab files. Using scripts written in house (Matlab, R2015a),

LFPs recorded within CA1 and in CA1 and PFC were analyzed for the magnitude squared coherence (Matlab function code: mscohere).

Immunocytochemistry and dendritic spine quantification

Rat hippocampal neurons (DIV 21) at low density were fixed by 4% PFA, permeabilized by 0.1% Triton X-100, and immuno-stained for synaptic proteins and visualized using a confocal fluorescence microscope. Anti-PSD95 (1:100; Santa Cruz Biotechnology), anti-Synapsin I (1:200; Cell signaling) antibodies and DAPI (Roche) were used. Synaptic clusters were calculated as the average number of clusters per 10 μm of dendritic length. AAV1-YFP was used to highlight dendritic spines of hippocampal neurons (DIV 21) at low density. Dendritic spines of primary and secondary basilar dendrites were counted and analyzed. Images were captured under a confocal microscope (Olympus).

Synaptosomal preparation and RNA analysis (qRT-PCR)

Total RNA was extracted from cells by using Trizol reagent (Life Technology). For synaptosomal RNA, pooled mouse hippocampi were homogenated into 10 volumes of ice cold HEPES-buffered sucrose (0.32 M sucrose, 4 mM HEPES pH 7.4) containing a RNase inhibitor. Centrifuge the homogenate at 1000 x g at 4°C to remove the pelleted nuclear fraction (P1) and unbroken cells. The resulting supernatant (S1) from further centrifugation at 10,000 x g for 15 min at 4°C yielded the crude synaptosomal pellet (P2). P2 was resuspended into 0.32 M sucrose and layered onto 4 ml of 1.2 M sucrose. Centrifuge at 38,000 rpm in SW51 and collect gradient interphase. Synaptosomal interphase was diluted with 0.32 M sucrose and then carefully layered onto 4 ml of 0.8 M sucrose. Centrifuge again to pellet synaptosomes. The pellet was then lysed in Trizol for RNA preparation. The High-Capacity cDNA Reverse Transcription Kit (Appliedbiosystems) was used to synthesize the first strand cDNA from the samples with an equal amount of RNA. Synthesized cDNAs were then amplified and analyzed on Real-Time PCR Systems (Invitrogen) using SYBR Green MasterMix (5 Prime). Primers used were listed in Supplementary Table 2.

Histology and Immunohistochemistry

Mice were heart-perfused by saline and 4% PFA, postfixed in 4% PFA overnight. Mouse brains were paraffin-embedded and 5 μm sections were deparaffinized by passing through 100% xylene and rehydrated through serial dilutions of ethanol (100, 95, and 75%). Hematoxylin and Eosin (H&E) staining was performed and images were captured under a light microscope. For OCT embedding, perfused brains were cryoprotected by 30% sucrose infiltration and then sectioned at 10 μm using a cryostat (Leica). Anti-HSF1 (1:100; cell signaling), anti-β-Amyloid (clone 4G8; 1:100; Covance), anti-NeuN (1:100; Millipore), anti-GFAP (1:1000; Sigma), anti-Iba1 (1:500; Wako) antibody was used and nuclei were stained with DAPI.

Protein analysis by Western blots

Western blots were performed as previously described[16]. Antibodies (Abs) were used as follows: rabbit anti-HSP90, cHSP70, HSP40, HSP27, HSF1, PSD95, Synapsin I (1:1000; Cell Signaling); mouse anti-iHSP70 (1:1000; Enzo Life Sciences), rabbit anti-BDNF (1:500;

Santa Cruz Biotechnology); mouse anti-β-actin (1:10000; Sigma-Aldrich), rabbit anti-Synaptophysin (1:2000; Chemicon/Millipore), and anti-mouse IgG and anti-rabbit IgG horseradish peroxidase-conjugated Abs (1:5000; Sigma-Aldrich).

Amyloid-beta ELISA

Cortex tissues were collected and processed using mouse amyloid beta 40 ELISA kit and amyloid beta 42 ELISA kit (Thermofisher) following the manufacture's protocol, with additional guanidine HCl to extract insoluble amyloid from tissues.

Behavior tests

Contextual fear conditioning—Contextual fear conditioning test was conducted as previous described[14]. Freezing percentage was analyzed by FreezeFrame software (Coulbourn Instruments).

Open field test—Each animal was individually placed in a novel open-field arena (47 L × 37 W × 20 H, cm; 900 lux at the center; Accuscan Instruments) for 10 min while being recorded by an overhead camera. Total locomotor activity was measured by beam breaks of the equipped 16 infrared beams. The footage was then analyzed by an automated tracking system (EthoVision XT software). The time spent in the center (25% of the field) was measured as a potential indicator for anxiolytic behavior.

Elevated Plus Maze (EPM)—The EPM apparatus is a "+"-shaped maze with two facing open arms, two facing closed arms and a center area (arm/wall sizes: 50 L × 10 W × 30 H, cm; Runway height from floor: 55 cm). Each mouse was allowed to freely explore the maze for 5 min. The preference for being in open arms over closed arms (expressed as a percentage of time spent in the open arms) was calculated to measure anxiety-like behavior.

Novel object recognition—The task is conducted in an open arena (47 L × 37 W × 20 H) with 2 objects in HSF1 heterozygous mice. During habituation (day 1), mice were allowed to freely explore the arena. On day 2, mice were exposed to 2 identical objects (red cubes) placed in the center of field. On day 3, 1 object was placed by another novel object (blue triangle). Each test lasted for 10 minutes. Time spent in exploring each object was recorded. Exploration time and discrimination index were calculated.

Cross Maze—Spontaneous alternation rates were assessed using a cross-maze. Cross maze was conducted in a "+"-shaped maze with four white and opaque plastic arms with walls (arm/wall sizes: 50 L × 10 W × 30 H, cm). This test is conducted based on the same principle and protocol as the Y-maze. Briefly, animals were introduced from a fixed entry located in one of the four arms, and were allowed to freely explore four arms for 5 min. An alternation is defined as going into each of the four arms without repeating an arm. Divide the number of alternations by the number of arm choices minus three to get the alternation rate, which is the measure of working memory.

Morris Water Maze—Water maze was conducted in a 118-cm diameter round tank, filled with 25 °C opaque water using non-toxic white tempera paint (Crayola). During the test,

mice were first trained to learn swimming and to find cued (visible by a black acrylic ball 30 cm above the platform) escape platform (10 cm diameter; 0.5 cm above water surface) for 3 days, then underwent 10 days of hidden platform session (0.5 cm below water surface) and 1 additional day of probe trial session (platform removed). Two days of rest were given before mice went to hidden platform session. During the hidden platform session, swimming path and distance was recorded and calculated as measures of spatial and learning memory. During the probe trial session, platform crossings and time spent in a 40-cm zone centered on the former platform location were recorded as measures of spatial memory.

Statistical Analysis

All statistical analysis was performed by Student's t-test for two groups' comparison, or one way ANOVA, followed by Tukey's (HSD) *post-hoc* tests for three or more groups' comparison. All quantitative data are presented by means ± s.e.m. The asterisks indicate significant difference versus control as follows: $*P < 0.05$, $**P < 0.01$ and $***P < 0.001$.

Results

OS47720 effectively induces activation of hippocampal HSF1 and the expression of synaptic proteins *in vivo*

The Pochoxime series of Hsp90-inhibiting compounds were reported to display feasible CNS-permeability and minimal systemic toxicity in reducing glioma progression upon 3-month treatment in mice[17–19]. We compared the prototypic geldanamycin (GA, systemically toxic) and 17-AAG (limited CNS permeability) with Pochoxime C (OS47720) (Figure 1a) for hepatotoxicity, each at 100 mg/kg via a single i.p. injection. The mice receiving GA died within 24 h while the remaining mice continued receiving daily injections of 17-AAG or OS47720. By the 5th day, 3/4 of the mice receiving 17-AAG demonstrated signs of severe lethargy and organ damage, while Hematoxylin and Eosin (H&E) staining showed no traceable hepatic and nephric alterations with OS47720 (Figure 1b and Supplementary Figure 1).

Neuronal exposure to 100 nM of OS47720 induced nuclear translocation, indicating rapid HSF1 activation, as similarly seen with 17-AAG[14] (Supplementary Figure 2). This was followed by sustained induction of multiple HSPs and synaptic markers with effects lasting 24–48 h (Supplementary Figure 3). Confocal microscopy demonstrated that OS47720 also caused a nearly 2-fold increase in synapsin I and PSD95 clusters and significantly protected synapses against soluble Aβ-impaired structural damage (Supplementary Figure 4).

Using LC-MS, we found that 1 h after a single intraperitoneal (i.p.) injection at 100 mg/kg, OS47720 reached a maximum concentration in the brain of ~ 1000 ng/g and declined rapidly over the next 2–24 h (Figure 2a). To determine the duration of OS47720's effects in mouse brain after a single i.p. injection, we measured induction of iHsp70 and PSD95 levels in various tissues over two days (Figure 2b). Although the iHsp70 protein is most abundant in skeletal muscle, Hsp90 inhibition elicited the greatest response in liver, as evidenced by the most dramatic induction of iHsp70 shown at 2 h. The hippocampi expressed much lower levels of iHsp70 from Hsp90 inhibition, although PSD95 was markedly elevated. It should

be noted that lumbar cord tissue did not demonstrate a response to the Hsp90 inhibitor, which is consistent with the idea of failed stress response in motor neurons/ALS mice as previously reported[8]. We also observed a long-lasting OS47720 effect on HSF1 nuclear translocation, most prominently as an increase in the HSF1 immunoreactivity in the pyramidal neurons of CA1, in cytoplasm and nuclei (DAPI/blue), peaking starting from 24 h, and, to a lesser degree in neurons of the CA3 region and cortex (Figure 2c). We confirmed that the HSF1 induction is indeed transcriptionally active by injecting OS47720 i.p. to young iHsp70 promoter-mPlum reporter mice[20]. This induced a long-lasting activation of the iHsp70 promoter, again most prominently in the CA1 regions and maintaining kinetics identical to those of HSF1 (Supplementary Figure 5), although the response was weaker than that in liver. Despite a relatively weak heat shock-like stress response, the induction of synaptic proteins is strong and long-lasting in hippocampi. These findings imply a potentially important role of HSF1 in hippocampally-mediated functions such as learning and memory.

OS47720 promotes dendritic spine formation in cortex and coherence of local field potential in hippocampus

Memory is closely associated with dendritic spine dynamics (including elimination and formation) in long-term memory[21, 22]. Using transcranial two-photon microscopy, we examined the effect of OS47720 on the dynamics of postsynaptic dendritic spines of Layer V pyramidal neurons in the motor cortex of Thy1-YFP-H line mice (Figure 3a). We found that in young adult mice, a single i.p. injection of OS47720 significantly increased the rate of spine formation (12.9 ± 1.2% versus 6.7 ± 0.5%, $P < 0.001$) over 2 days. No significant difference in spine elimination was observed between OS47720 - and vehicle-treated animals (8.1 ± 1.3% versus 7.8 ± 0.8%, $P = 0.660$) (Figure 3b, c). These results indicate that OS47720 was effective in promoting synapse formation *in vivo,* an idea which is consistent with our *in vitro* findings (Supplementary Figure 4e, f).

To determine whether OS47720 could functionally affect neuronal activity in memory-related hippocampal and cortical-hippocampal networks of aged mice, we performed simultaneous extracellular recordings of local field potentials (LFPs) in the prefrontal cortex (PFC) and hippocampal CA1 region of 18-month old mice. Two electrodes (spaced 0.3 mm apart) were placed in CA1 and one electrode in the PFC (Supplementary Figure 6a). This allowed assessment of coherence of neuronal activity within CA1 and between the PFC and CA1. Here we analyzed coherence of LFP activity for three 10 min time windows: immediately before and after OS47720 or vehicle treatment and 24 h after treatment.

In our recordings in CA1 characteristic sharp-wave-ripple (SWR) complexes[23] were frequently observed and were synchronized between the two recording locations (Figure 3d–f). The presence of SWRs, was used to identify CA1 recording locations during experiments. Recording sites were also confirmed anatomically for a subset of mice using small electrolytic lesions placed at the end of recording sessions (Supplementary Figure 6b). Coherence of LFP activity was compared before and after OS47720 or vehicle infusion. Immediately following OS47720 or vehicle treatment, there were no significant effects of OS47720 on coherence (Figure 3g–i). However, 24 h after treatment coherence in CA1 was

significantly increased for frequencies between 20–30 Hz and 110–120 Hz (Figure 3g). There also was a trend for LFP coherence in CA1 to be elevated across all frequency bands tested (1–220 Hz). Vehicle injection did not affect coherence within CA1 at either of the two post-injection time points (Figure 3h).

Functional interactions between CA1 and PFC have been studied extensively, particularly in the context of memory formation[24–26]. We measured the coherence, the degree of phase-locking of oscillatory neuronal activity at two recording sites corresponding to these two brain structures that has been most implicated in cognitive processes. In the OS47720-treated group, LFP coherence between the CA1 and PFC was significantly increased at frequencies between 190–200 Hz and decreased at frequencies between 70–80 Hz (Figure 3i). Vehicle injection had no effect on coherence between the CA1 and PFC (Supplementary Figure 6c).

Chronic treatment with OS47720 rescues spatial learning and memory in acute Aβ and symptomatic Tg2576 mice

The therapeutic effect of OS47720 was first evaluated in an acute model of Aβ-impaired contextual conditioned freezing memory. In young C57BL/6 mice, Aβ (from 7PA2 conditioned medium[14]) was administered 5 days after daily OS47720 injection, three times via intracerebroventricular (i.c.v.) injection through the implanted cannula at the indicated time points (Supplementary Figure 7a). The acquisition of freezing behavior was recorded during the first day of training, and the contextual fear retention was recorded 24, 48 and 72 h later. OS47720 treatment improved contextual freezing memory, reaching statistical significance at the 72 h time point (Supplementary Figure 7b). Protein analysis revealed restored PSD95 and mature BDNF following OS47720 treatment (Supplementary Figure 7c, d). Profiling of various BDNF isoforms indicated that Aβ reduced the majority of BDNF isoforms in hippocampal synaptosomes, while they were largely rescued by OS47720, some even restored to a higher level when compared to the control (Supplementary Figure 8).

We then tested OS47720 (100 mg/kg i.p. every two days for 3 months) on early symptomatic Tg2576 and littermate control mice starting from 9 months of age. This dosage was determined based on a previous study[19] and our dosing experiment on B6 mice. Over the course of treatment there was no significant weight loss and no group differences in weight gain (Supplementary Figure 9a, b). Moreover, there were no group differences on any measure of locomotor activity or anxiety (Supplementary Figure 10). Working memory was greatly impaired in the Tg2576 group, as indicated by significantly lower alternation rate on the cross maze test, and this was almost completely rescued by OS47720 (Figure 4a, b).

The Morris water maze test was used to measure spatial and learning memory. Distance was used as a dependent measure because of a slightly (but non-significant) faster swimming speed in the Tg-Vehicle group, compared to the other three groups. Mice in all groups readily found the cued platform (Figure 4c). On the hidden-platform training, there were significant effects of genotype and drug, and a significant Genotype x Drug interaction. Vehicle-treated Tg mice were significantly impaired relative to their Non-Tg counterparts (Figure 4c), consistent with previous reports in these mice[27]. OS47720 treatment rescued this spatial learning impairment in the Tg group, demonstrated by significantly shorter swim

paths. OS47720 treatment did not improve spatial learning and memory in the non-Tg mice and there was no genotypic difference in the OS47720 -treated mice (Figure 4c). A probe trial was conducted 24 h after the last hidden-platform session to assess memory for the former platform location. Time spent in a 40-cm zone centered on the former platform location was used as an index of spatial memory as it was a more precise measure in the target quadrant (Figure 4e). The vehicle-treated transgenic mice did not spend significantly more time in the target zone, when compared to the mean of the other three zones (Figure 4d). Similarly, these mice did not discriminate between the former platform location and equivalent positions in the other three quadrants. In contrast, mice in the other three groups showed a selective search for the targets. Heat maps show a more defined swim path in OS47720 -treated groups, indicating superior spatial reference memory (Figure 4f). Consistent with our *in vitro* data, the expression levels of iHsp70, synaptic proteins (synapsin I and PSD95, but not SNAP25), and BDNF, were significantly increased in the hippocampi of Tg2576 mice after chronic OS47720 treatment (Figure 4g, h).

We repeated OS47720 testing on mid-stage symptomatic Tg2576 from 12 months to 18 months of age and observed very similar results. There was a slight decrease in body weight (10–14% on males and 5–12% on females) over a 6-month treatment course in all vehicle and OS47720 treatment groups, suggesting mild toxicity or stress caused by the vehicle (Supplementary Figure 9c, d). Similar to the previous results, the deficit of working memory in the Tg-Veh group was again significantly improved by OS47720 treatment in Tg mice, with no difference in total entries among all groups (Figure 4i, j). The Morris water maze test revealed impaired long-term spatial learning and memory in the Tg-Veh group, which was significantly improved in the Tg-OS47720 group to the point where memory was comparable to that of the non-Tg and non-Tg-Veh groups (Supplementary Figure 4k). During probe trial sessions, the Tg-Veh group lacked preference in the target search, while the other three groups selectively searched for the target zone (Supplementary Figure 4l). Vehicle treatment had no effect on cross maze or Morris water maze tests (Supplementary Figure 7i–l). Similarly, chronic OS47720 treatment again rescued the expression levels of HSPs (iHSP70, HSP40), PSD95 and BDNF (Figure 4m, n). Notably, HSF1 expression was also rescued by OS47720 in both cohorts to a level even higher than that of non-Tg (Figure 4g, m). End-point studies of Aβ (4G8) levels revealed that OS47720 did not significantly reduce Aβ plaques (immunofluorescence staining) or soluble and insoluble Aβ (ELISA) or neuroinflammation (stained with astrocytes maker GFAP and microglia maker Iba1) in the brain after chronic treatment (Supplementary Figure 11), nor did the levels of transthyretin[28] differ among all four groups (Supplementary Figure 12). Taken together, OS47720 improved memory, including short term working memory and long term spatial and learning memory, in both early and mid-stage Tg2576 mice.

OS47720 exhibits neuroprotection and memory amelioration via HSF1

We hypothesized that OS47720 improves memory through activation of HSF1. We firstly microinjected an HSF1-specific pharmacological inhibitor, KRIBB11[29], into mice at various time points during fear training. Strikingly, triple injections of KRIBB11 impaired contextual memory even more severely than did Aβ administration (Figure 5a, b). This was accompanied by marked reductions of HSF1, HSPs, and various synaptic proteins (Figure

5c, d). Overexpression of a constitutively active hsf1 (AAVH-BH)[30] or AAV-shRNA*hsf1* to downregulate hsf1 by AAVs resulted in opposite consequences of heat shock response (e.g., iHsp70), synaptic proteins (PSD95) and BDNF (Figure 5e, f). Furthermore, The AAV-mediated downregulation of HSF1, specifically in the hippocampal region and DG (Figure 5g), diminished contextual memory at both 48 and 72 h after training which could not be rescued by OS47720 (Figure 5h, i). In contrast, OS47720-treated mice had slightly higher basal contextual memory at these time points. An end-point study of the altered proteins revealed abolished HSP40, PSD95, and mature BDNF by AAVshRNAhsf1 administration; changes that were not restored by OS47720 treatment (Figure 5j, k). In addition, HSF1 heterozygous knockout mice showed impaired working memory, recognition memory, and locomotor activity, but not anxiety (Supplementary Figure 13). These results indicate that HSF1 plays a significant role in memory and that the beneficial effects of OS47720 require functionally active HSF1. To determine whether requirement of HSF1 is more prevalent in the initial stage of memory acquisition and consolidation or for all stages (including retrieval and extinction), we administered KRIBB11 at 1 h before and 1, 3, 6, 8, and 24 h after training. The most significant abrogating effect was observed at 1 h post-training, and to a lesser degree at 3 and 6 h post-training. No effect was observed when injected at 8 or 24 h post-training (Supplementary Figure 14). These results indicate that HSF1 is required for the initial stage of memory consolidation or retrieval.

OS47720 effect is mediated by activated CREB bypassing cAMP/PKA and PI3K/Akt pathways

To determine whether OS47720 induced BDNF upregulation via the classic cAMP-PKA-CREB pathway, cAMP levels were measured in cultured hippocampal neurons. OS47720 did not alter intracellular cAMP production even when a priming concentration of forskolin was included (Supplementary Figure 15a). The lack of a role of the cAMP-PKA-CREB, MAPK, and PI3K pathways in the formation of dendritic spines was confirmed by pharmacological inhibitors (i.e., RpcAMP and H89, U0126 and LY294002; Supplementary Figure 15b)., These results are consistent with our previous reports showing reduced Akt levels upon Hsp90 inhibition in neurons[18]. A CaMKII inhibitor did reduce the effect of OS47720 on dendritic spines. Statistical analysis revealed significant loss of dendritic spines using KN93, a selective CaMKII inhibitor, with or without co-treatment of OS47720, while no effect was observed by using its inactive derivative, KN92 (Supplementary Figure 15c).

Discussion

While Hsp90 inhibitors have been investigated as anti-cancer agents over the past 2 decades[31, 32], and as therapeutic agents for neurodegenerative diseases over the past decade[3, 4], they have yet to demonstrate any clinical success. In addition to systemic toxicity, brain penetrability represents another major challenge for therapeutic development of the drug for CNS applications. Although there is evidence of two CNS-permeable Hsp90 inhibitors successfully reducing tau aggregation with feasible toxicity profiles, they were tested either too acutely (single i.p. injection)[33] or too briefly (7 days)[6]. Herein, we have presented data demonstrating successful chronic (6 months) treatment of symptomatic Tg2576 mice with a CNS-permeable and non-toxic Hsp90 inhibiting compound. Notably,

we demonstrate a unique mechanism of Hsp90 inhibition in preserving synaptic structures and functions. The potential therapeutic implications of these findings are boundless, and are only further encouraged by the remarkable pharmacokinetics and pharmacodynamics of this compound (OS47720).

In the past decade, the stress response to heat or Hsp90 inhibitors is generally considered blunted in neurons[34, 35]. While much of the data were generated through neuroblastoma or rodent primary neuronal culture models, there is a dearth of *in vivo* data until recently[36]. Our *ex vivo* data (Supplemental Figure 5b) on the iHsp70 reporter mice after either single or continual OS47720 treatment also indicate a relatively weakened, but not blunted, neuronal HSF1/iHsp70 response in the brain relative to the liver and muscle. It was observed that the hippocampal CA1 region (versus CA3) demonstrated the greatest HSF1/iHsp70 response, while spinal cord motor neurons demonstrated almost undetectable responses (Figure 2b). This finding is consistent with previous reports that motor neurons have a high threshold for activation of HSP genes, which may explain why this neuronal type is the most vulnerable and undergoes the most rapid degeneration[8]. There are several possibilities for the weak HSRs in neurons, which may not be mutually exclusive: 1) the presence of intrinsic repressor(s) at the HSE sites 2) HSF1 itself is differently regulated in neurons; 3) the existence of intrinsically inert neuronal *iHSP70* promoter. Hippocampal CA1 region has long been recognized to be most vulnerable to stress response (e.g., ischemia) presumably due to the “glucocorticoid oversensitivity”[37], the most prominent HSF1 activation in CA1 may represent neuronal attempt to perverse the most important functions rendered by this subregion. These possibilities warrant further investigation.

In addition to heat-shock proteins, our work highlights HSF1-mediated transcriptional upregulation of multiple synaptic genes, which include genes coding for synapsin I, synaptophysin, PSD95, BDNF, as well as several immediate early genes (IEGs). Based on the consensus sequences of HSF1-binding elements (HSEs), we identified potential HSEs in the promoter regions of these genes (Supplementary Tab. 2). Among them, we provide evidence of direct binding of HSF1 to an HSE1 site in close vicinity to the key CREB binding site (CRE) in *bdnf* promoter I, which was upregulated 1 h post-foot shock. Additionally, several IEGs were also induced at this time point. Surprisingly, the expression of SNAP-25, a member of the SNARE family and synaptosomal-associated protein of 25 KD at presynapses, was not reduced in 12 MO Tg2576 mouse brain (Fig. 4g), nor its expression was upregulated by HSF1. Together, these results imply that HSF1 is another principle transcriptional factor which is required for gene upregulation during consolidation or retention of fear contextual memory via its interplay with CREB. This concept is also supported by the data demonstrating significant abrogating effects of the HSF1 inhibitor administered 1 h post-training (Supplemental Figure 14). We believe that HSF1 plays a regulatory role in reshaping the synaptic transcriptome on a genomic scale (Supplemental Figure 16), which ultimately contributes to neurodegeneration. Indeed, the HSF1-regulated transcriptome was found to be impaired by an aggregated huntingtin (Htt) protein, which may participate in the neurodegeneration observed in Huntington’s disease[38].

OS47720 mediates its therapeutic effect in Tg2576 mice via highly novel synaptic strengthening mechanisms via modulation of HSP90. The unique sustained (> 3 d) induction

of synaptic genes/protein expression after a single i.p. injection of OS47720 may be attributed to multiple mechanisms, including transcriptional regulation. This is not surprising given the large pool (> 800) of cellular proteins identified as Hsp90 client proteins, many of which may include membrane receptors necessary for neuronal transmission (e.g., AMPAR)[39] as well as proteins regulating posttranscriptional microRNAs and translational processes. Indeed, we observed markedly enhanced spine formation 24–48 h following a single injection of OS47720, which was confirmed by 2-photon microscopic live imaging in young mice. Notably, we demonstrated that in healthy aged mice (18 months) OS47720 alters coherence of LFP activity within the hippocampal CA1 region and between CA1 and the prefrontal cortex for beta (12 – 30Hz), gamma (30 – 100Hz) and higher frequency (190 – 200 Hz) oscillations. Coherence measures the degree of phase-locking of oscillatory neuronal activity at two recording sites and is an indicator of neuronal communication between brain structures that has been implicated in cognitive processes[40–42]. Abnormalities in coherence of brain activity have been shown to be associated with AD, both in humans[43, 44] and a mouse model[45] of the disease. It has been proposed that measures of coherence of brain activity could serve as a biomarker for AD[46, 47]. LFP coherence between the PFC and CA1 within the gamma frequency range has been strongly implicated in attention, working memory and memory consolidation[26, 48]. Our findings suggest that the rescue of memory deficits by OS47720 treatment observed in AD mice is indicative of OS47720 effecting coherent neuronal activity between the PFC and CA1.

Neurodegenerative diseases are commonly characterized by aberrant formation of pathological protein aggregates. While the clearance of misfolded proteins following Hsp90 inhibition is ill-defined, it is generally accepted that it requires induction of a heat shock-like response that results in HSF1-mediated upregulation of other chaperone proteins such as iHsp70 and its co-chaperones (e.g., Hsp40/DNAJ and Hsp27 etc). Of note, OS47720 did not cause any observable effects in reducing amyloid Aβ load in Tg2576 mice after 3- or 6-month-treatments, despite various reports of anti-Aβ effects by other Hsp90 inhibitors[49, 50]. These seemingly contradictory results reflect intrinsic differences between *in vitro* and *in vivo* experimental systems, as the majority of reports indicating Aβ-reducing effects were derived from *in vitro* studies which lack the proper neuroglial microenvironment. We believe that the lack of Aβ reduction after chronic OS47720 administration is due to the modest induction of stress responsive proteins (iHsp70 and Hsp40) by this drug (Figure 4g, h. m, n). While it has been acknowledged that high levels of iHsp70 (and perhaps other co-chaperones) facilitate Aβ degradation[51], such as in the cases of Hsp70 overexpression in AD mice crossed with an Hsp70 transgenic[52, 53] or DNAJ (Hsp40) overexpression on Htt degradation in R6/2 mice[54], it appears that such high expression levels of chaperone proteins is not achievable via Hsp90 inhibition in mice.

HSF1 dysregulation in neurodegeneration is largely unstudied. In aged Tg2576 mice, we found significantly reduced (~ 20 %) protein expression of HSF1 in the hippocampi relative to their non-Tg littermates (Figure 4g, h, m, n). Chronic OS47720 treatment not only normalized HSF1 expression, but also elevated basal levels of expression. That an Hsp90 inhibitor can upregulate the HSF1 gene and its expression has not yet been reported. We have evidence supporting the role of an Hsp90 inhibitor upregulating the *hsf1* gene in neurons (Liao, unpublished data). We recently discovered that loss of HSF1 protein is due to

UPS-mediated protein degradation in primary patient brains with Lewy's bodies. This was caused by proteotoxic stresses from misfolded and aggregated proteins such as α-synuclein, which may contribute to α-synucleinopathy[55]. Although soluble Aβ can also induce HSF1 degradation in neuronal cellular cultures, as well as in APP-overexpressing FAD transgenic mice, the extent of HSF1 loss is not as severe as in the cases of ALS, alpha-synuclein, or R6/2 Htt transgenic mice (Liao, unpublished data).

HSF1 is the most important master stress response regulator, yet its role and regulatory mechanisms in CNS disease remains ill-defined. Our restudy has sought to address this void in neurodegenerative research. HSF1 expression levels are reduced in the granule Purkinje neurons in AD rat cerebellum, and AAV-delivered HSF1 into the brain stem reversed neurodegeneration[56]. We believe that pharmacological agents that can activate and stabilize HSF1 protein expression and function hold therapeutic promise for treating a chronic neurodegenerative disease such as AD. Among the four currently-known CNS-permeable Hsp90 inhibitors[6–8, 33], OS47720 is the only Hsp90 inhibitor compound that has demonstrated exceptional *in vivo* performance in AD mice, including an apparent lack of systemic toxicity at therapeutically-relevant dosage over a chronic period of time (see summary in Supplementary Table 3). The notion of currently limited success with the other CNS-permeable compounds prompts us to consider a potential fundamental difference between AD and other neurodegenerative diseases (i.e., PD, HD and ALS). It appears that AD is more of a synaptic disease[57, 58] than one caused by severe proteinopathy, an idea that becomes more attractive when considering the 2–3 decade window of chronic neurodegeneration in AD compared to a less than 2 year disease onset of an ALS patient. Our work is the first demonstrating feasibility of treating a chronic dysfunctional synaptic disease such as AD with a pharmacologically feasible Hsp90 inhibitor (OS47720). Most notably, it is effective on treating symptomatic mice with significant amyloid plaque load via protecting synapses. Hence, this work demonstrates translational significance. In particular, by combining Hsp90 inhibitor-mediated synaptic protection with other anti-amyloid treatment (e.g., β-secretase inhibitors), it may offer a viable treatment option for treating symptomatic AD patients.

Supplementary Material

Refer to Web version on PubMed Central for supplementary material.

Acknowledgments

We thank Drs. William E Armstrong (Anatomy & Neuroscience UTHSC) and Melloni Cook (University of Memphis) for valuable inputs, Dr. Deborah Young (The University of Auckland, Auckland, New Zealand) for providing constitutively expressed AAVH-HB hsf1 viruses[28]; Tonia Rex (Vanderbilt University) for AAV-shRNA viral vector. This work is supported by NIH grants to F-F L. (AG049772-01); D.H.H. (NS091752); M P. M. (AG040230 & AG041935); G. Y. (GM107469; AG048410); W. Li. (CA148706); K. S. (MH105567 and MH102445); R. O. (GM107094). D.H.H. also received support from the UTHSC College of Medicine iRISE Pilot Program. Some of the behavioral procedures were conducted at the Neuroscience Institute's Behavioral Core at UTHSC.

References

1. Becker RE, Greig NH, Giacobini E. Why do so many drugs for Alzheimer's disease fail in development? Time for new methods and new practices? J Alzheimers Dis. 2008; 15:303–325. [PubMed: 18953116]
2. Honig LS. Translational research in neurology: dementia. Arch Neurol. 2012; 69:969–977. [PubMed: 22473767]
3. Luo W, Sun W, Taldone T, Rodina A, Chiosis G. Heat shock protein 90 in neurodegenerative diseases. Mol Neurodegener. 2010; 5:24. [PubMed: 20525284]
4. Neef DW, Jaeger AM, Thiele DJ. Heat shock transcription factor 1 as a therapeutic target in neurodegenerative diseases. Nat Rev Drug Discov. 2011; 10:930–944. [PubMed: 22129991]
5. Putcha P, Danzer KM, Kranich LR, Scott A, Silinski M, Mabbett S, et al. Brain-permeable small-molecule inhibitors of Hsp90 prevent α-synuclein oligomer formation and rescue α-synuclein-induced toxicity. J Pharmacol Exp Ther. 2010; 332:849–857. [PubMed: 19934398]
6. Dickey CA, Kamal A, Lundgren K, Klosak N, Bailey RM, Dunmore J, et al. The high-affinity HSP90-CHIP complex recognizes and selectively degrades phosphorylated tau client proteins. J Clin Invest. 2007; 117:648–658. [PubMed: 17304350]
7. Labbadia J, Cunliffe H, Weiss A, Katsyuba E, Sathasivam K, Seredenina T, et al. Altered chromatin architecture underlies progressive impairment of the heat shock response in mouse models of Huntington disease. J Clin Invest. 2011; 121:3306–3319. [PubMed: 21785217]
8. Cha JR, St Louis KJ, Tradewell ML, Gentil BJ, Minotti S, Jaffer ZM, et al. A novel small molecule HSP90 inhibitor, OS47720 30001, differentially induces heat shock proteins in nervous tissue in culture and in vivo. Cell Stress Chaperon. 2014; 19:421–435.
9. Stetler RA, Gan Y, Zhang W, Liou AK, Gao Y, Cao G, et al. Heat shock proteins: cellular and molecular mechanisms in the central nervous system. Prog Neurobiol. 2010; 92:184–211. [PubMed: 20685377]
10. Moon IS, Park IS, Schenker LT, Kennedy MB, Moon JI, Jin I. Presence of both constitutive and inducible forms of heat shock protein 70 in the cerebral cortex and hippocampal synapses. Cereb Cortex. 2001; 11:238–248. [PubMed: 11230095]
11. Morimoto RI. Regulation of the heat shock transcriptional response: cross talk between a family of heat shock factors, molecular chaperones, and negative regulators. Genes Dev. 1998; 12:3788–3796. [PubMed: 9869631]
12. Zou J, Guo Y, Guettouche T, Smith DF, Voellmy R. Repression of heat shock transcription factor HSF1activation by HSP90 (HSP90 complex) that forms a stress-sensitive complex with HSF1. Cell. 1998; 94:471–480. [PubMed: 9727490]
13. Taipale M, Jarosz DF, Lindquist S. HSP90 at the hub of protein homeostasis: emerging mechanistic insights. Nat Rev Mol Cell Biol. 2010; 117:515–528.
14. Chen Y, Wang B, Liu D, Li JJ, Xue Y, Sakata K, et al. Hsp90 chaperone inhibitor 17-AAG attenuates Aβ-induced synaptic toxicity and memory impairment. J Neurosci. 2014; 34:2464–2470. [PubMed: 24523537]
15. Yang G, Pan F, Parkhurst CN, Grutzendler J, Gan W-B. Thinned-skull cranial window technique for long-term imaging of the cortex in live mice. Nat Protoc. 2010; 5:201–208. [PubMed: 20134419]
16. Wang R, Li JJ, Diao S, Kwak YD, Liu L, Zhi L, et al. Metabolic stress modulates Alzheimer's β-secretase gene transcription via SIRT1-PPARγ-PGC-1 in neurons. Cell Metab. 2013; 17:685–694. [PubMed: 23663737]
17. Barluenga S, Fontaine JG, Wang C, Aouadi K, Chen R, Beebe K, et al. Inhibition of HSP90 with pochoximes: SAR and structure-based insights. Chembiochem. 2009; 10:2753–2759. [PubMed: 19856365]
18. Wang C, Barluenga S, Koripelly GK, Fontaine JG, Chen R, Yu JC, et al. Synthesis of pochoxime prodrugs as potent HSP90 inhibitors. Bioorganic & medicinal chemistry letters. 2009; 19:3836–3840. [PubMed: 19410458]

19. Zhu H, Woolfenden S, Bronson RT, Jaffer ZM, Barluenga S, Winssinger N, et al. The novel Hsp90 inhibitor NXD30001 induces tumor regression in a genetically engineered mouse model of glioblastoma multiforme. Mol Cancer Ther. 2010; 9:2618–2626. [PubMed: 20643786]
20. de la Rosa X, Santalucía T, Fortin PY, Purroy J, Calvo M, Salas-Perdomo A, et al. *In vivo* imaging of induction of heat-shock protein-70 gene expression with fluorescence reflectance imaging and intravital confocal microscopy following brain ischaemia in reporter mice. Eur J Nucl Med Mol Imaging. 2013; 40:426–438. [PubMed: 23135322]
21. Kasai H, Fukuda M, Watanabe S, Hayashi-Takagi A, Noguchi J. Structural dynamics of dendritic spines in memory and cognition. Trends Neurosci. 2010; 33:121–129. [PubMed: 20138375]
22. Yang G, Pan F, Gan W-B. Stably maintained dendritic spines are associated with lifelong memories. Nature. 2009; 462:920–924. [PubMed: 19946265]
23. Buzsáki G, Buhl DL, Harris KD, Csicsvari J, Czéh B, Morozov A. Hippocampal network patterns of activity in the mouse. Neuroscience. 2003; 116:201–211. [PubMed: 12535953]
24. Yu JY, Frank LM. Hippocampal-cortical interaction in decision making. Neurobiol Learn Mem. 2015; 117:34–41. [PubMed: 24530374]
25. Brincat SL, Miller EK. Frequency-specific hippocampal-prefrontal interactions during associative learning. Nat Neurosci. 2015; 18:576–581. [PubMed: 25706471]
26. Spellman T, Rigotti M, Ahmari SE, Fusi S, Gogos JA, Gordon JA. Hippocampal-prefrontal input supports spatial encoding in working memory. Nature. 2015; 522:309–314. [PubMed: 26053122]
27. Westerman MA, Cooper-Blacketer D, Mariash A, Kotilinek L, Kawarabayashi T, Younkin LH, et al. The relationship between Abeta and memory in the Tg2576 mouse model of Alzheimer's disease. J Neurosci. 2002; 22:1858–1867. [PubMed: 11880515]
28. Wang X, Cattaneo F, Ryno L, Hulleman J, Reixach N, Buxbaum JN. The systemic amyloid precursor transthyretin (TTR) behaves as a neuronal stress protein regulated by HSF1 in SH-SY5Y human neuroblastoma cells and APP23 Alzheimer's disease model mice. J Neurosci. 2014; 34:7253–7265. [PubMed: 24849358]
29. Yoon YJ, Kim JA, Shin KD, Shin DS, Han YM, Lee YJ, et al. KRIBB11 inhibits HSP70 synthesis through inhibition of heat shock factor 1 function by impairing the recruitment of positive transcription elongation factor b to the hsp70 promoter. J Biol Chem. 2011; 286:1737–1747. [PubMed: 21078672]
30. Jung AE, Fitzsimons HL, Bland RJ, During MJ, Young D. HSP70 and constitutively active HSF1 mediate protection against CDCrel-1-mediated toxicity. Mol Ther. 2008; 16:1048–1055. [PubMed: 18398426]
31. Neckers L. Hsp90 inhibitors as novel cancer chemotherapeutic agents. Trends Mol Med. 2002; 8:S55–61. [PubMed: 11927289]
32. Whitesell L, Lindquist SL. HSP90 and the chaperoning of cancer. Nat Rev Cancer. 2005; 5:761–772. [PubMed: 16175177]
33. Luo W, Dou F, Rodina A, Chip S, Kim J, Zhao Q, et al. Roles of heat-shock protein 90 in maintaining and facilitating the neurodegenerative phenotype in tauopathies. Proc Natl Acad Sci US A. 2007; 104:9511–9516.
34. Marcuccilli CJ, Mathur SK, Morimoto RI, Miller RJ. Regulatory differences in the stress response of hippocampal neurons and glial cells after heat shock. J Neurosci. 1996; 16:478–485. [PubMed: 8551332]
35. Batulan Z, Shinder GA, Minotti S, He BP, Doroudchi MM, Nalbantoglu J, et al. High threshold for induction of the stress response in motor neurons is associated with failure to activate HSF1. J Neurosci. 2003; 23:5789–5798. [PubMed: 12843283]
36. Carnemolla A, Lazell H, Moussaoui S, Bates GP. In vivo profiling reveals a competent heat shock response in adult neurons: implications for neurodegenerative disorders. PLoS One. 2015; 10:e0131985. [PubMed: 26134141]
37. Riva L, Koeva M, Yildirim F, Pirhaji L, Dinesh D, Mazor T, et al. Poly-glutamine expanded huntingtin dramatically alters the genome wide binding of HSF1. J Huntingtons Dis. 2012; 1:33–45. [PubMed: 23293686]
38. Conrad CD. Chronic stress-induced hippocampal vulnerability: the glucocorticoid vulnerability hypothesis. Rev Neurosci. 2008; 19:395–411. [PubMed: 19317179]

39. Gerges NZ, Tran IC, Backos DS, Harrell JM, Chinkers M, Pratt WB, et al. Independent functions of hsp90 in neurotransmitter release and in the continuous synaptic cycling of AMPA receptors. J Neurosci. 2004; 24:4758–4766. [PubMed: 15152036]
40. Bastos AM, Vezoli J, Bosman CA, Schoffelen JM, Oostenveld R, Dowdall JR, et al. Visual areas exert feedforward and feedback influences through distinct frequency channels. Neuron. 2015; 85:390–401. [PubMed: 25556836]
41. Buzsaki G, Schomburg EW. What does gamma coherence tell us about inter-regional neural communication? Nat Neurosci. 2015; 18:484–489. [PubMed: 25706474]
42. Fries P. Rhythms for Cognition: Communication through Coherence. Neuron. 2015; 88:220–235. [PubMed: 26447583]
43. Chen CC, Hsu CY, Chiu HW, Hu CJ, Lee TC. Frequency power and coherence of electroencephalography are correlated with the severity of Alzheimer's disease: A multicenter analysis in Taiwan. J Formos Med Assoc. 2013; 114:729–735. [PubMed: 23969043]
44. Hsiao FJ, Wang YJ, Yan SH, Chen WT, Lin YY. Altered oscillation and synchronization of default-mode network activity in mild Alzheimer's disease compared to mild cognitive impairment: an electrophysiological study. PLoS One. 2013; 8:e68792. [PubMed: 23874766]
45. Liu Q, Li A, Gong L, Zhang L, Wu N, Xu F. Decreased coherence between the two olfactory bulbs in Alzheimer's disease model mice. Neurosci Lett. 2013; 545:81–85. [PubMed: 23628669]
46. Sankari Z, Adeli H, Adeli A. Wavelet coherence model for diagnosis of Alzheimer disease. Clin EEG Neurosci. 2012; 43:268–278. [PubMed: 22715491]
47. Basar E, Basar-Eroglu C, Guntekin B, Yener GG. Brain's alpha, beta, gamma, delta, and theta oscillations in neuropsychiatric diseases: proposal for biomarker strategies. Suppl Clin Neurophysiol. 2013; 62:19–54. [PubMed: 24053030]
48. Benchenane K, Tiesinga PH, Battaglia FP. Oscillations in the prefrontal cortex: a gateway to memory and attention. Curr Opin Neurobiol. 2011; 21:475–485. [PubMed: 21429736]
49. Lu Y, Ansar S, Michaelis ML, Blagg BS. Neuroprotective activity and evaluation of Hsp90 inhibitors in an immortalized neuronal cell line. Bioorg Med Chem. 2009; 17:1709–1715. [PubMed: 19138859]
50. Ansar S, Burlison JA, Hadden MK, Yu XM, Desino KE, Bean J. A non-toxic Hsp90 inhibitor protects neurons from Abeta-induced toxicity. Bioorg Med Chem Lett. 2007; 17:1984–1990. [PubMed: 17276679]
51. Magrané J, Smith RC, Walsh K, Querfurth HW. Heat shock protein 70 participates in the neuroprotective response to intracellularly expressed beta-amyloid in neurons. J Neurosci. 2004; 24:1700–1706. [PubMed: 14973234]
52. Hoshino T, Suzuki K, Matsushima T, Yamakawa N, Suzuki T, Mizushima T. Suppression of Alzheimer's disease-related phenotypes by expression of heat shock protein 70 in mice. J Neurosci. 2011; 31:5225–5234. [PubMed: 21471357]
53. Bobkova NV, Garbuz DG, Nesterova I, Medvinskaya N, Samokhin A, Alexandrova I, et al. Therapeutic effect of exogenous hsp70 in mouse models of Alzheimer's disease. J Alzheimers Dis. 2014; 38:425–435. [PubMed: 23985416]
54. Labbadia J, Novoselov SS, Bett JS, Weiss A, Paganetti P, Bates GP, et al. Suppression of protein aggregation by chaperone modification of high molecular weight complexes. Brain. 2012; 135:1180–1196. [PubMed: 22396390]
55. Kim E, Wang B, Sastry N, Masliah E, Nelson PT, Cai H, et al. NEDD4-mediated HSF1 degradation underlies α-synucleinopathy. Hum Mol Genet. 2016; 25:211–222. [PubMed: 26503960]
56. Jiang YQ, Wang XL, Cao XH, Ye ZY, Li L, Cai WQ. Increased heat shock transcription factor 1 in the cerebellum reverses the deficiency of Purkinje cells in Alzheimer's disease. Brain Res. 2013; 1519:105–111. [PubMed: 23665061]
57. Palop JJ, Mucke L. Amyloid-β–induced neuronal dysfunction in Alzheimer's disease: from synapses toward neural networks. Nat Neurosci. 2010; 13:812–818. [PubMed: 20581818]
58. Koffie RM, Hyman BT, Spires-Jones TL. Alzheimer's disease: synapses gone cold. Mol Neurodegener. 2011; 6:63. [PubMed: 21871088]

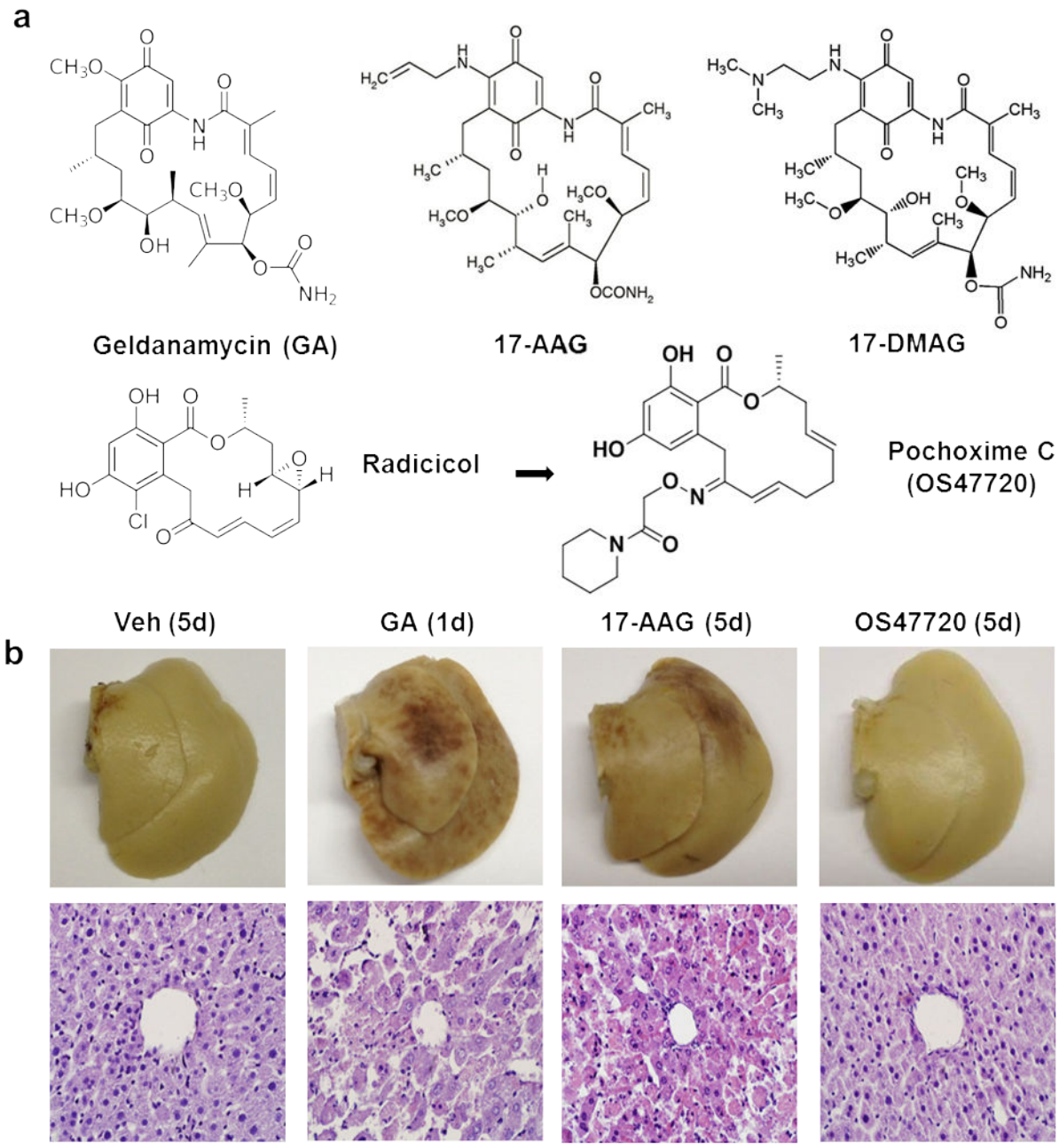

Figure 1.

Compound structures and toxicity. (**a**) Chemical structures of geldnanamycin, 17-AAG, 17-DMAG, radicicol and pochoxime C. (**b**) Representative images of whole liver morphology and H&E staining.

a **OS47720 Brain Concentrations**

Time point	Mouse	ng/g	Time point	Mouse	ng/g	Time point	Mouse	ng/g	Time point	Mouse	ng/g
1h	Mouse1	760.5	**2h**	Mouse6	643.2	**6h**	Mouse9	126.9	**24h**	Mouse12	4.4
	Mouse2	1016.2		Mouse7	308.2		Mouse10	92.1		Mouse13	2.5
	Mouse3	1035.5		Mouse8	290.6		Mouse11	147.2		Mouse14	2.7
	Mouse4	947.7								Mouse15	3.1
	Mouse5	954.0									
Mean ± STD		**942.8 ± 108.8**			**414.0 ± 198.7**			**122.1 ± 27.9**			**3.2 ± 0.9**

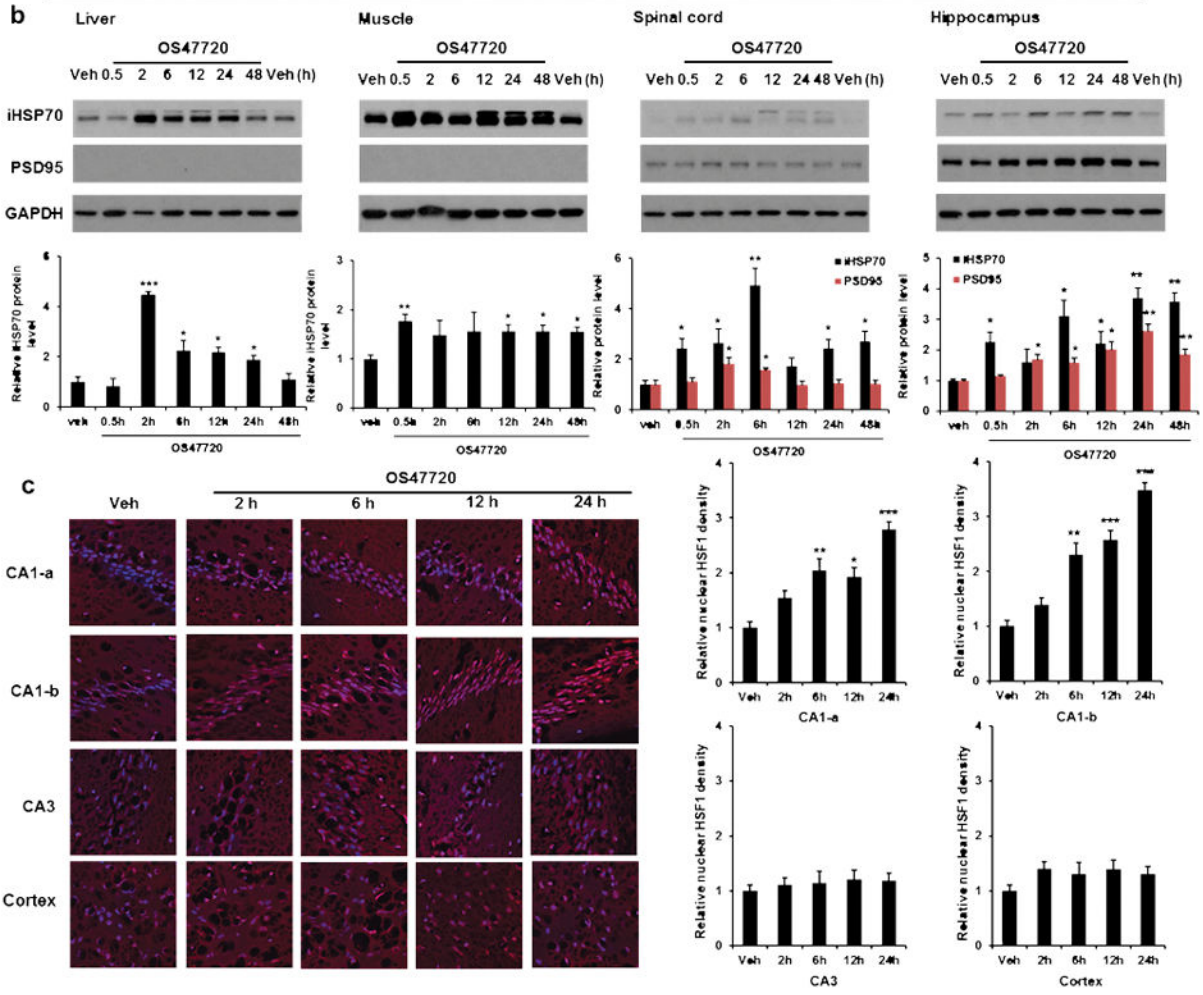

Figure 2.

Pharmacokinetics and pharmacodynamics of OS47720. (**a**) Brain concentrations of OS47720 detected by LC-MS/MS after i.p. injection at 100 mg/kg. (**b**) Mouse liver, skeletal muscle, lumbar spinal cord, and hippocampi were collected at 6 different time points after i.p. injection of OS47720 at 100 mg/kg. Western blot analyses detecting inducible HSP70 (iHSP70), PSD95, and GAPDH were performed. Histogram below shows statistical analysis. n = 3. (**c**) Representative images of HSF1 immunohistochemistry (red) of the four different regions and subregions of mouse brain (Hippocampal CA1-a, CA1-b, CA3 and

cerebral cortex), with nuclei stained with DAPI (blue). Images were captured by a confocal microscope at 600X magnification. n = 3. One-way ANOVA followed by *Tukey's Post-Hoc* test, all groups vs Veh, $*P < 0.05$, $**P < 0.01$ and $***P < 0.001$. Data represent mean ± s.e.m.

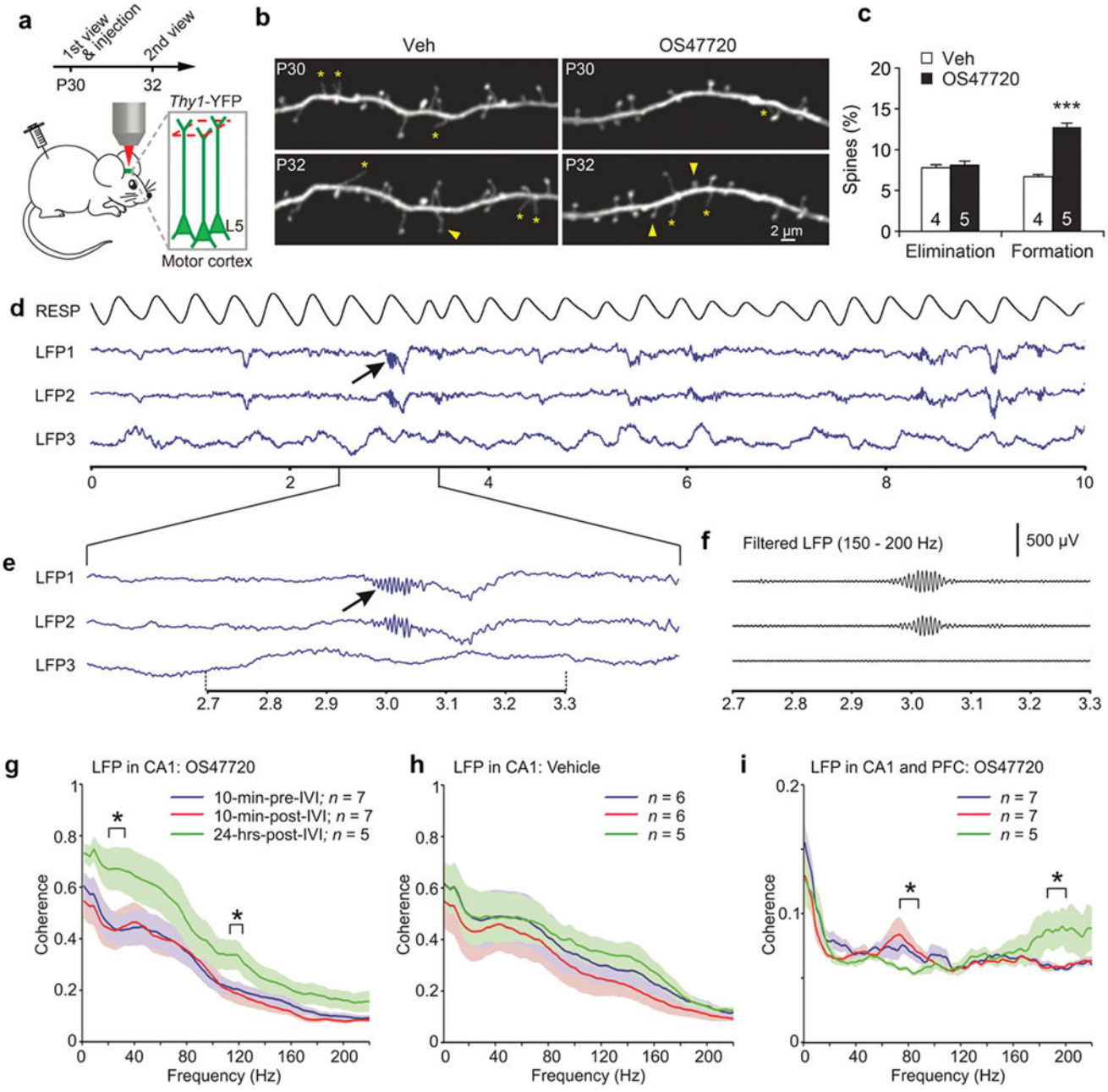

Figure 3.

OS47720 increases dendritic spine formation by *in vivo* imaging and neuronal activity by *in vivo* recordings. (**a**) Schematic illustration of the timeline of OS47720 administration and *in vivo* imaging in Thy1-YFP mice. (**b**) Transcranial two-photon imaging of dendritic spines in the motor cortex of Veh- and OS47720 -treated mice. Filled arrowheads indicate spines that were formed between the two views. Asterisks indicate filopodia. Scale bar, 2 μm. (**c**) The percentages of spines that were formed or eliminated over 2 days in Veh- and OS47720 -treated mice. A significant increase in spine formation was found in OS47720-treated mice (***$P < 0.001$, n = 5 mice for OS47720 group, n = 4 mice for vehicle group). Data are

presented as mean ± s.e.m. (**d**) Raw data examples of local field potentials (LFPs) recorded from the CA1 region of the hippocampus (LFP1, LFP2) and from the PFC (LFP3) in awake, head-fixed mice. The uppermost trace shows respiration related temperature changes (RESP) with inspiration corresponding to an increase in voltage. The arrow in the LFP1 trace points at a characteristic high-frequency ripple in the CA1-LFP activity. Abscissa represents time in seconds. Amplitude scale bar shown in (f) applies to LFP traces in d–f. (**e**) Enlarged view of raw LFPs around the hippocampal ripple event marked by the arrow in (d). (**f**) Band-pass filtered versions of the LFP traces in panel (**e**) emphasizes the high-frequency ripple components of CA1 activity. (**g, h**) Coherence of LFP activity recorded from two sites within the hippocampal CA1 region of OS47720 and vehicle groups, respectively. Coherence was calculated for 10 minute data segments recorded immediately before (blue traces) and immediately after injections (red traces) and 24 h after injections (green traces). Brackets mark frequency bands where OS47720 treatment significantly altered CA1 LFP coherence compared to pre-injection control (*$P < 0.05$, two-sample t-test: comparisons between pre- and 1-day-post OS47720/vehicle). Vehicle treatment had no effect on CA1 LFP coherence. (**i**) LFP coherence between CA1 and PFC. Trace color codes are the same as in (**g, h**). Brackets are as in (g) and mark frequencies where OS47720 treatment significantly altered coherence of CA1-PFC LFP activity. Coherence data are expressed in mean ± s.e.m.

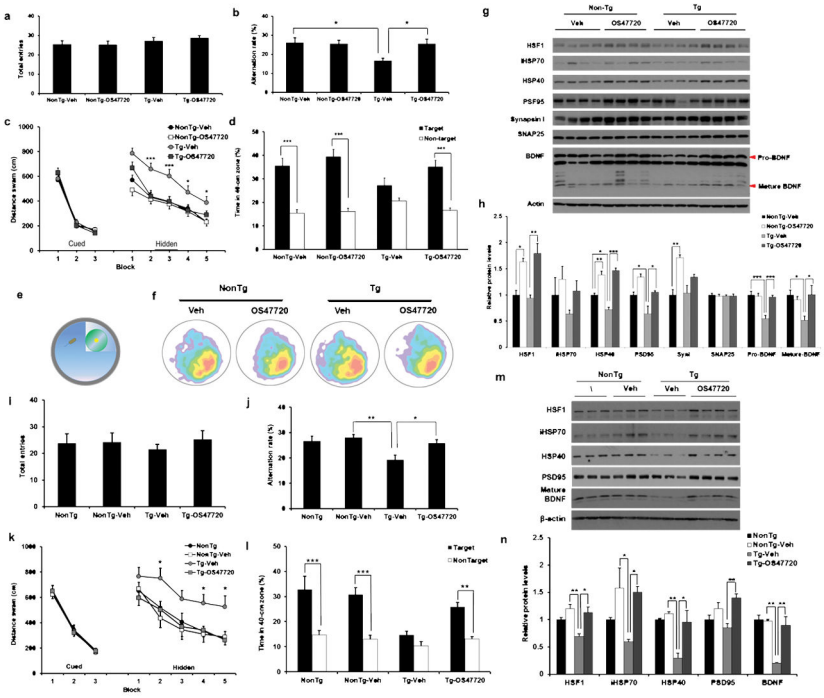

Figure 4.

Therapeutic Efficacy of chronic OS47720 in AD mouse model and the molecular changes at the end point. (**a–h**) Effects on early symptomatic Tg2576 mice after 3-month treatment (9–12 months). n = 20–21. Each group includes half males and females: (**a**) Total entries in the cross maze. (**b**) Alteration rate (%) representing working memory on the cross maze was calculated as the number of alterations divided by (total entries-3)*100. (**c**) Distance swam was used in Morris water maze test to evaluate spatial and learning memory. Histogram represents distance swam (cm) in cued and hidden platform sessions. Distance was averaged every two days in the hidden platform sessions; (**d**) Time spent in target (40 cm) and non-target zones during probe session was analyzed among groups; (**e**) Schematic diagram shows target zone surrounding the location of the missing platform, as well as a non-target zone along the pool; (**f**) Representative images of the heat map from each experimental group during the probe session; (**g**) Representative images (4 mice from each group) of Western blot analysis after Morris water maze. HSF1, Heat shock proteins (iHSP70, and HSP40), synaptic proteins (PSD95, synapsin I, and SNAP25) and BDNF were tested in four groups; (**h**) Statistical analysis of the Western blot data presented in (g). n = 6. (**i–n**) Effects on mid-symptomatic Tg2576 mice after 6-month treatment (12–18 months). n = 11–13. Each group includes half males and females: (**i, j**) Total entries and alteration rate (%) representing working memory on cross maze calculated as above. (**k, l**) Morris water maze test in cued session, hidden platform session and probe trial session. (**m**, **n**) Western blot analysis on postmodern tissue followed by quantification. n = 5–6. One-way ANOVA followed by *Tukey's Post-Hoc* test, NonTg-Veh vs NonTg-OS47720, Tg-Veh vs NonTg-Veh, Tg-Veh vs Tg-OS47720, $*P < 0.05$, $**P < 0.01$ and $***P < 0.001$. Error bars show means ± s.e.m.

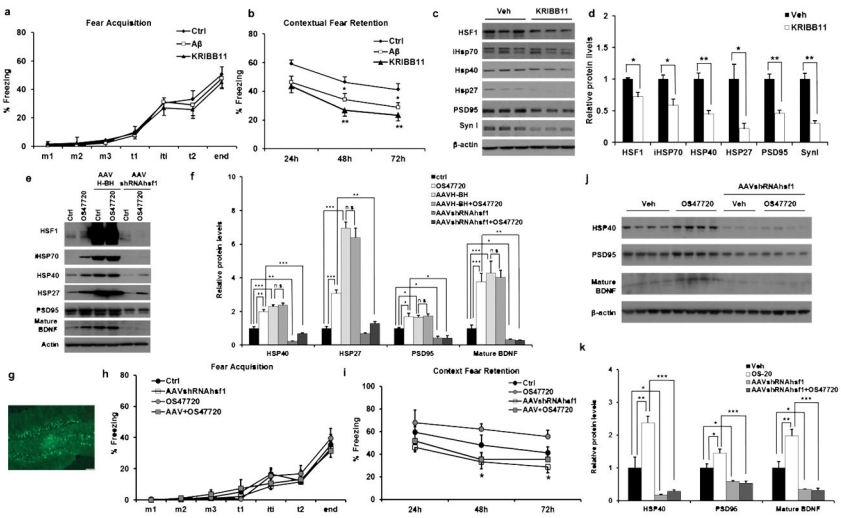

Figure 5.

HSF1 is required for memory. (**a**) Freezing time (%) during fear acquisition (training) in the contextual fear conditioning test. Ctrl, control. (**b**) Recorded contextual fear retention (context retrieval) 24, 48 and 72 h after training. One-way ANOVA followed by *Tukey's Post-Hoc* test, ctrl vs Aβ, $*P < 0.05$; ctrl vs KRIBB11, $**P < 0.01$. (**c**) Western blot analysis on the hippocampi of mice treated with the pharmacological inhibitor KRIBB11, 4 h after i.c.v. injection. Protein levels of HSF1, iHSP70, HSP40, HSP27, synapsin I and PSD95 were determined. n = 3. **(d)** Histogram shows the statistical analysis (Two-sample student t-test, $*P < 0.05$ and $**P < 0.01$). (**e**) AAVH-BH[29] (overexpressing constitutive active form of HSF1) and AAVshRNAhsf1 were introduced to cultured primary hippocampal neurons at 7–10 DIV. OS47720 (100 nM) was added 5–7 days after viral infection and was incubated for 24 hours. Western blot analysis was performed afterwards. (**f**) Statistical analysis of quantification using one-way ANOVA on 3 independent experiments, followed by *Tukey's post-hoc* test, all groups were compared with control except the AAVshRNAhsf1+OS47720 group, which was compared with OS47720. n.s., non-significant. n = 3. $*P < 0.05$, $**P < 0.01$ and $***P < 0.001$. (**g**) EGFP expression in mouse brain 14 days after AAVshRNAhsf1 was stereotactically microinjected into hippocampus. (**h, i**) Freezing time (%) during fear acquisition and contextual fear retention in the contextual fear conditioning test. n = 10–12. One-way ANOVA with Tukey's *post-hoc* test, ctrl vs AAVshRNAhsf1. $*P < 0.05$. (**j**) Representative images of Western blot analysis after contextual fear conditioning. (**k**) Statistical analysis of the Western blot data based. n = 6. One-way ANOVA with Tukey's *post-hoc* test, $*P < 0.05$ and $***P < 0.001$.